Doping-driven structural phase transition and loss of superconductivity in $M_xFe_{1-x}Se_\delta$ (M=Mn, Cu)

Tzu-Wen Huang,[1,*] Ta-Kun Chen,[1] Kuo-Wei Yeh,[1] Chung-Ting Ke,[1] Chi Liang Chen,[1] Yi-Lin Huang,[1] Fong-Chi Hsu,[1] Maw-Kuen Wu,[1,†] Phillip M. Wu,[2] Maxim Avdeev,[3] and Andrew J. Studer[3]

[1]*Institute of Physics, Academia Sinica, Nankang, Taipei, Taiwan*

[2]*Department of Physics, Duke University, Durham, North Carolina 27708, USA*

[3]*Bragg Institute, Australian Nuclear Science and Technology Organisation, PMB 1, Menai, New South Wales 2234, Australia*

(Received 19 August 2009; revised manuscript received 23 July 2010; published 2 September 2010)

In this paper, we report the results of detailed studies on Mn and Cu substitution to Fe site of β-FeSe, namely, $Mn_xFe_{1-x}Se_{1-\delta}$ and $Cu_xFe_{1-x}Se_{1-\delta}$ (δ equals to 0.03–0.05 based on our neutron-diffraction refinements). The results show that with only 10 at. % Cu doping the compound becomes a Mott insulator. Detailed temperature-dependent structural analyses of these Mn- and Cu-substituted compounds show that the structural transition, which is associated with the changes in the building block $FeSe_4$ tetrahedron, is essential to the occurrence of superconductivity in β-FeSe.

DOI: 10.1103/PhysRevB.82.104502 PACS number(s): 74.62.Bf, 74.70.Ad

The iron-pnictide[1–6] and β-FeSe (Refs. 7–9) superconductors have become a focus of condensed-matter research in the past year. In the parent iron selenide superconductors, there exists a structural transition at temperature (Ts) much higher than the superconducting transition point (Tc). At Ts the tetragonal lattice ($P4/nmm$) distorts into a lower symmetry monoclinic lattice ($P112/n$) (or orthorhombic with the defined a-b plane rotated about 45° with respect to the original lattice). In both the LaFeAsO (1111) and $BaFe_2As_2$ (122) families it was suggested that this phase transition, which is accompanied with an antiferromagnetic state developed at around the same temperature, has to be suppressed either by chemical doping or applying external pressure in order to observe superconductivity.[5,10–14] However, this distortion seems to be indispensable to the superconductivity in the FeSe (11) compound.[7,15–18] Preliminary Mössbauer measurements[19,20] suggested no magnetic ordering developed below Ts and beyond Tc in FeSe. On the other hand, strong spin fluctuation below the structural distortion temperature has been observed in NMR (Refs. 21–23) and spin-resonance (SR) (Ref. 24) experiments.

In order to further investigate the distortion issue, substitutions on Fe sites were studied earlier in 11,[16] and in the 1111 (Ref. 25) and 122 families.[14,26,27] Among all substituent alternatives, transition metals, especially those with unpaired 3d electrons such as Mn, Co, Ni, and Cu,[28] would be of most interest for their comparable ionic sizes to Fe, and the potential to investigate in more detail the interplay between magnetism and superconductivity, which may also lead to better insight into the origin of superconductivity in this class of materials.

Preliminary results on a series of 3d transition-metal-substituted $FeSe_{1-x}$ compounds were reported in an earlier publication.[16] For all 3d elements (from Ti to Cu) with 10 at. % substitution, we found only Mn, Co, Ni, and Cu could retain the tetragonal structure. We later decided to investigate in detail the $Cu_xFe_{1-x}Se_{1-\delta}$ and $Mn_xFe_{1-x}Se_{1-\delta}$ samples for comparison as we found only 3 atomic percent (at. %) Cu doping completely suppressed superconductivity whereas up to 5.5 at. % Mn substitution only slightly decreased the superconducting transition temperature.

Cu- and Mn-substituted samples were prepared with method reported earlier.[16] Transmission electron microscopy (TEM) analysis was performed on powder samples suspended on gold grids coated with amorphous carbon in a JEOL 2100F transmission electron microscope equipped with scanning transmission electron microscopy (STEM) and energy-dispersive x-ray spectroscopy (EDX) spectral analytical parts. The x-ray absorption near edge spectra were measured with calibrated standard iron foil at BL16A NSRRC with energy resolution about 0.1 eV. Cell parameters were calculated from the experiments performed in synchrotron source (BL12b2 at SPring 8 and BL13A at NSRRC) with an incident beam of wavelength 0.995 Å. Neutron powder diffraction data were collected using Echidna and Wombat diffractometers[29,30] at the OPAL reactor, Australia. The samples were loaded in 6 mm cylindrical vanadium cans and data were collected in the temperature range 3–300 K using wavelength of 1.885 Å. The resistance measurements were carried out using the standard four-probe method with silver paste for contacts.

Figure 1 shows the temperature dependence of electrical resistivity of $Cu_xFe_{1-x}Se_{1-\delta}$ and $Mn_xFe_{1-x}Se_{1-\delta}$ compounds with various x values. Our results showed that Mn doping only has limited solubility up to about 5 at. %. On the other hand, the Mn doping seems to persist even up to about 30 at. %. However, detailed composition analysis by near edge of diffraction anomalous fine structure shows that there are only 2.2 ± 1.1 at. % to 5.5 ± 1.1 at. % Mn substituted at iron site in those samples with nominal 10–30 at. % Mn doping. Superconducting transition in $Cu_xFe_{1-x}Se_{1-\delta}$ [Fig. 1(a)] was observed only in samples with $x \leq 0.02$. For $x \geq 0.03$, the compound gradually becomes nonmetallic.[28] Detailed analysis of the temperature dependence of resistivity shows that for 10 at. % Cu-doping sample the resistivity, as shown in the inset of Fig. 1(a), fits well with the three-dimensional Mott variable range hopping transport. In contrast, $Mn_xFe_{1-x}Se_{1-\delta}$ [Fig. 1(b)] remains metallic and superconducting for x as high as 0.055 with only very little variation in Tc, as shown in the inset of Fig. 1(b).

 ©2010 The American Physical Society

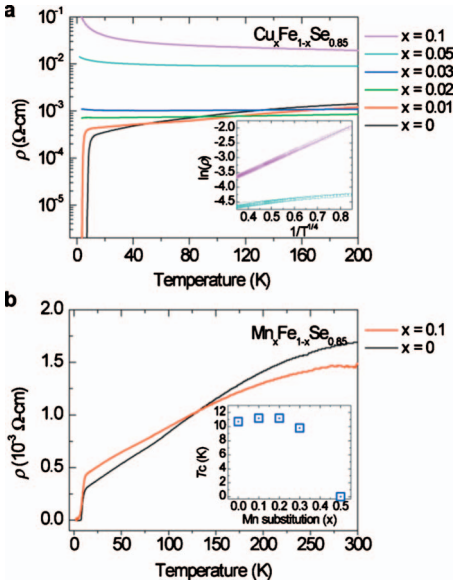

FIG. 1. (Color) (a) Temperature-dependent electrical resistivity (ρ) at zero magnetic field for bulk $Cu_xFe_{1-x}Se_{1-\delta}$ (x=0, 0.01, 0.02, 0.03, 0.05, and 0.1) samples. Inset shows the low-temperature resistivity plotted against $1/T^{1/4}$ (b) Temperature dependence of electrical resistivity for bulk $Mn_xFe_{1-x}Se_{1-\delta}$ (x=0 and 0.022, in nominal composition) samples. Inset shows Tc as a function of Mn substitution.

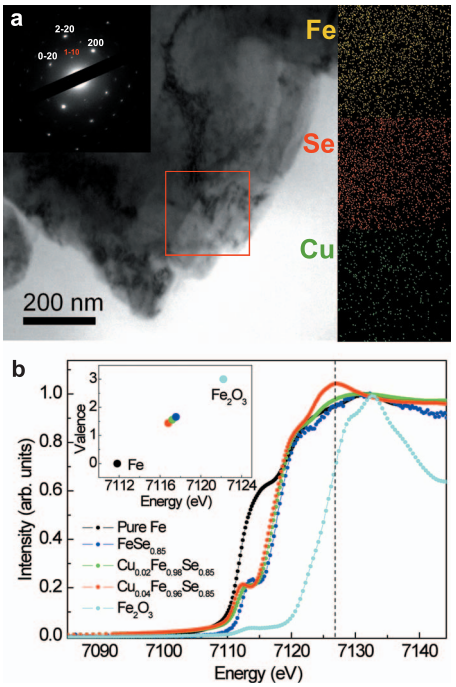

FIG. 2. (Color) (a) The bright field TEM image and the corresponding selected-area electron diffraction of $Cu_{0.04}Fe_{0.96}Se_{1-\delta}$ powder sample, aligned along the (001) direction revealing the fourfold symmetry of the tetragonal structure. The reflection marked by red indexes is expected to be very weak due to systematic abscence. At the right side we present the STEM/EDX elemental mappings of the area of interest marked by a red square using a 2 Å electron probe, which demonstrate the random distribution of copper in the sample. (b) The x-ray absorption near-edge structure (XANES) in Fe K edge for $Cu_xFe_{1-x}Se_{1-\delta}$($x$=0–0.04), Fe foil (upper), and FeO (bottom). The inset plots the valence states of Fe, which are calculated from the first derivative of the XANES spectra.

It was surprising that only 3 at. % Cu doping makes the sample become an insulator. Figure 2(a) shows a TEM image of a $Cu_{0.04}Fe_{0.96}Se_{1-\delta}$ powder sample along the sample c axis. The selected-area electron diffraction shows that there are strong reflections at the (hkl), $h+k=2n$, $h=k$=odd positions, which are expected to be very weak in FeSe. This strongly suggests the successful substitution of Cu into Fe site. The 2 Å scanning electron probe of STEM/EDX elemental mappings, which is smaller than the Fe-Fe or Se-Se distance, is expected to be able to resolve any clustering or nonuniformity in the samples. The results, shown in the right panel of Fig. 2(a), of the area of interest marked by a red square demonstrate no particular feature of copper in the sample suggesting homogeneous dispersion of Cu over the whole sample. The Fe and Se concentrations are as well found uniformly distributed in the sample.

The XAS Fe K-edge spectra are shown in Fig. 2(b), which are normalized at the photon energy ~100 eV from the absorption edge at E_0=7112 eV (pure Fe). The feature marked as a1 is mainly due to the transition from Fe 1s to the 4sp state as in the $FeSe_x$ series.[31] A comparison of the spectra of the standard (Fe and FeO) and the $Cu_xFe_{1-x}Se_{1-\delta}$ samples with x=0–0.04 reveals the energy shifting at the a1 regions around 7116.8 eV with increasing x value. The results indicate that the variation in Fe valence, which is shown in the inset of Fig. 2(b), decreases from +1.81 at x=0 to +1.66 at x=0.04. The linear shifting of absorption edge gives additional support to the random distribution of Cu over Fe, since inhomogeneity may give rise to deviations in the absorption spectra. In the Fe 4p states,[32] a smooth feature from 8 to 15 eV above the edge also showed a tendency toward larger areas, suggesting a systematic increase in unoccupied states above the Fermi level as more Cu is substituted. These results may provide a rational explanation to the observed resistivity increases and eventual insulating behavior, in higher Cu-doping samples.

In Fig. 3 we show the schematic crystal structure of β-FeSe and the temperature-dependent neutron powder diffraction (NPD) patterns of Cu- and Mn-substituted samples. Figure 3(b) is the temperature dependence of neutron scattering for $Cu_{0.01}Fe_{0.9}Se_{1-\delta}$ (left) and $Cu_{0.1}Fe_{0.9}Se_{1-\delta}$ (right) bulk samples. Peak splitting was observed in (220), (221), and (114) reflections at ~60 K in the $Cu_{0.01}Fe_{0.9}Se_{1-\delta}$ sample. However, no splitting could be identified for any peak in $Cu_{0.1}Fe_{0.9}Se_{1-\delta}$ sample from 140 to 10 K, indicating the absence of any structural distortion in the 10 at. % Cu-doping samples. The typical refinement for NPD results of 10% Cu-doped FeSe sample is shown at Fig. 3(c).

On the other hand, in the NPD of $Mn_{0.01}Fe_{0.99}Se_{1-\delta}$ (left) and $Mn_{0.022}Fe_{0.978}Se_{1-\delta}$ (right) bulk samples, Fig. 3(d), peak splitting is observed in (220), (221), and (114) reflections at ~85 K and ~62 K, respectively, indicating the onset of structural phase transition. This phase transition could be described by a structural distortion from tetragonal lattice ($P4/nmm$) to monoclinic ($P112/n$), which is much the same

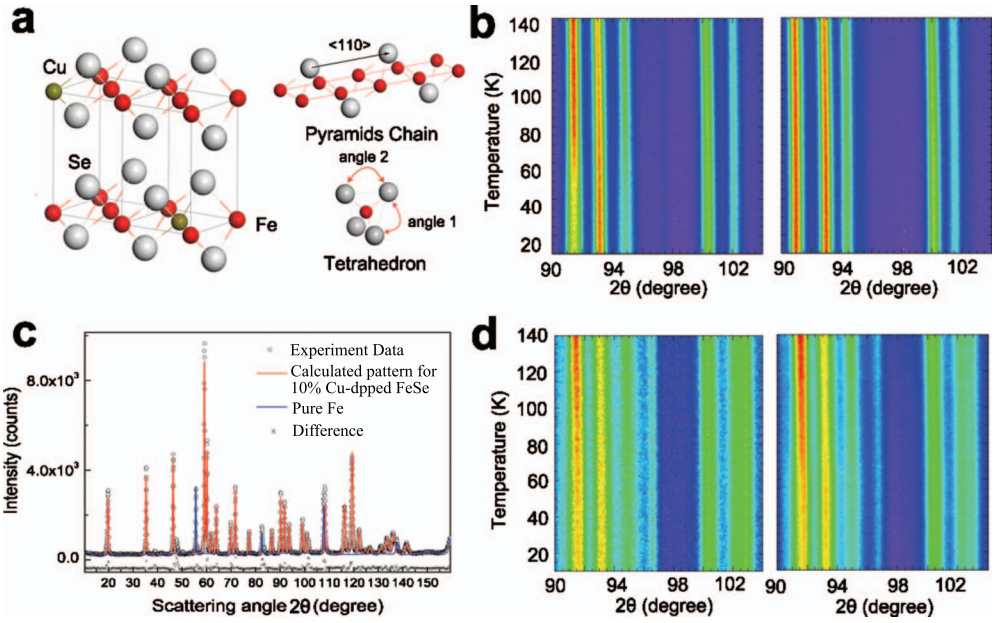

FIG. 3. (Color) (a) Crystal structure of $Cu_xFe_{1-x}Se_{1-\delta}$, sketched schematically with Fe in red, Cu in dark yellow, and Se in gray color. The pyramids chain and tetrahedron with respect to iron are shown to the right. (b) Temperature dependence of NPD for $Cu_{0.01}Fe_{0.9}Se_{1-\delta}$ (left) and $Cu_{0.1}Fe_{0.9}Se_{1-\delta}$ (right) bulk samples. (c) The typical refinement for NPD results of 10% Cu-doped FeSe sample. The calculated diffraction peaks for 10% Cu-doped FeSe is shown as the red line and the blue line shows the impurity phase pure Fe. The difference between the experimental data and the sum of calculated patterns is shown as cross mark. (d)The NPD of $Mn_{0.01}Fe_{0.99}Se_{1-\delta}$ (left) and $Mn_{0.022}Fe_{0.978}Se_{1-\delta}$ (right). Similar structural change is observed as evidenced by the peak splitting in (220), (221), and (114) reflections at ~85 K and ~62 K, respectively.

as observed in the FeSe (Refs. 7 and 33) and $FeSe_{0.5}Te_{0.5}$ at temperatures below ~100 K.[8] Moreover, if viewing along the (110) direction, the lattice that distorts from tetragonal to monoclinic does not destroy the magnetic symmetry, allowing superconductivity to occur.[8]

Detailed Rietveld refinements of the diffraction data give insight into the Cu substitution effect on the crystal structure of $Cu_xFe_{1-x}Se_{1-\delta}$. Rietveld refinements were carried out using GSAS software to confirm the accuracy and quality of results and also based on a model with anion vacancies model.[34–36] Not only the basic lattice parameters but also the Debye Waller factor, crystal size, and temperature dependence of lattice strain are considered. In Tables I and II, we list some fitting parameters, respectively, for copper concentration dependence and temperature dependence at 10% Cu doping. The lattice constants a and c were found slightly modified by Cu substitution, as shown in Figs. 4 and 5(a). In terms of the tetrahedron shown in Fig. 3(a), we found that that Cu doping causes shrinkage of the Fe-Se bond length and slight expansion in Fe-Fe bond length [Fig. 5(b)], which

TABLE I. The refinement results for Cu and Mn concentration dependence in FeSe.

M (%)	a, c	Occupancies (Fe:TM:Se)	Fractional coordinates of Se (x,y,z)	R_{wp}%, R_p% [a]
0% Cu	3.783(4), 5.543(3)	0.99(4):0.00(7):0.95(7)	(0,0.5,0.2604)	6.77%, 2.68 %
1% Cu	3.798(7), 5.543(5)	0.99(2):0.00(8):0.95(7)	(0,0.5,0.2606)	8.17%, 3.68 %
2% Cu	3.790(8), 5.504(1)	0.98(5):0.01(5):0.96(4)	(0,0.5,0.2629)	9.08%, 4.83 %
3% Cu	3.792(2), 5.508(9)	0.97(2):0.02(8):0.95(5)	(0,0.5,0.2621)	8.58%, 4.45 %
4% Cu	3.794(7), 5.511(6)	0.96(5):0.03(5):0.95(8)	(0,0.5,0.2615)	9.86%, 4.55 %
5% Cu	3.798(5), 5.509(5)	0.95(2):0.04(8):0.95(5)	(0,0.5,0.2502)	7.5 %, 3.8 %
10% Cu	3.841(7), 5.512(6)	0.88(9):0.11(1):0.95(7)	(0,0.5,0.2591)	9.31%, 5.49 %
1% Mn	3.773(3), 5.531(6)	0.98(8):0.01(2):0.94(1)	(0,0.5,0.2644)	3.41%, 2.55 %
2.2% Mn	3.766(3), 5.520(6)	0.97(8):0.02(2):0.95(7)	(0,0.5,0.2648)	4.15%, 3.11 %
3.6% Mn	3.727(2), 5.504(1)	0.96(4):0.03(6):0.96(5)	(0,0.5,0.2655)	3.05%, 2.01 %
5.5% Mn	3.699(4), 5.501(4)	0.94(5):0.05(5):0.94(2)	(0,0.5,0.2667)	4.02%, 2.71 %

[a]Reflex uses the weighted profile R factor and the profile R factor, R_{wp} and R_p, to measure the similarity between the simulated and the experimental diffraction patterns.

TABLE II. The refinement results for temperature concentration dependence in FeSe with 10% Cu.

Temperature, 10% Cu (K)	a, c in FeSe	Fractional coordinates of Se (x,y,z)	R_{wp}%, R_p% [a]
6	3.826(0), 5.486(4)	(0,0.5,0.2558)	7.41%, 4.27%
20	3.826(2), 5.486(9)	(0,0.5,0.2572)	9.12%,5.89%
50	3.826(4), 5.487(9)	(0,0.5,0.2577)	8.82%, 8.01%
100	3.827(9), 5.491(3)	(0,0.5,0.2573)	7.99%, 5.62%
200	3.833(8), 5.502(6)	(0,0.5,0.2570)	10.48%, 4.62%
250	3.837(2), 5.508(5)	(0,0.5,0.2532)	12.62%, 8.89%
300	3.841(7), 5.512(6)	(0,0.5,0.2591)	9.31%,5.49%

[a]Reflex uses the weighted profile R factor and the profile R factor, R_{wp} and R_p, to measure the similarity between the simulated and the experimental diffraction patterns.

is accompanied with changes in Se-Fe-Se bond angles [Fig. 5(c)]. These effects combined leads toward a regular tetrahedron (γ=109.28°), i.e., compression of the tetrahedron. This hardened bond strength could inhibit the structural transition at low temperature. Thus, the low-temperature structural transition (Ts) was drastically suppressed and eventually disappeared when the concentration of Cu substitution exceeded 3 at. %.

Our experimental observations can be summarized in the structural phase diagram as shown in Fig. 5(d) for

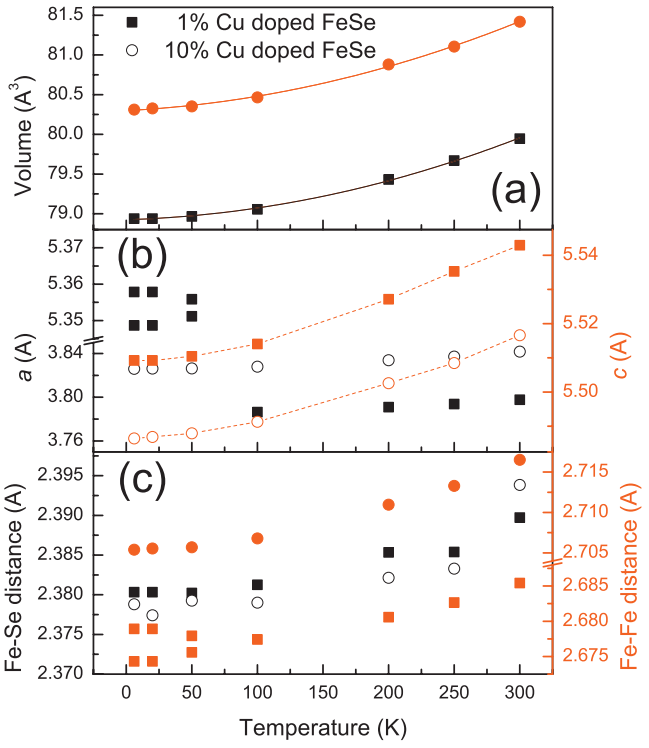

FIG. 4. (Color) The lattice parameters and detailed structure information, including (a) volume (b) a, c, and (c) Fe-Se, Fe-Fe distances, as temperature dependence in superconducting FeSe with 1% Cu doping and nonsuperconducting FeSe with 10% Cu doping.

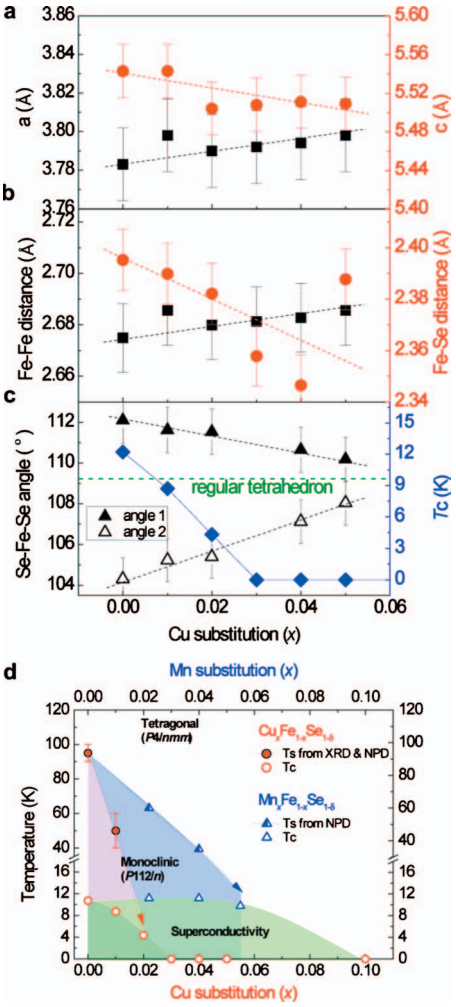

FIG. 5. (Color) [(a)–(c)] Lattice constants, Fe-Se and Fe-Fe bond lengths, Se-Fe-Se bond angles, and Tc of $Cu_xFe_{1-x}Se_{1-\delta}$ as a function of Cu substitution, x. (d) The structural phase diagrams of $Cu_xFe_{1-x}Se_{1-\delta}$ and $Mn_xFe_{1-x}Se_{1-\delta}$ determined from neutron and synchrotron x-ray powder diffraction data and resistivity data. The solid triangles and circles indicate the onset of tetragonal to monoclinic structural distortion, Ts, and the hollow triangles and circles designate the onset of superconductivity, Tc.

$Cu_xFe_{1-x}Se_{1-\delta}$ and $Mn_xFe_{1-x}Se_{1-\delta}$. The substitution by Cu or Mn on Fe site clearly drives down the structural transition temperature Ts, and it also reveals the correlation between Ts and Tc. As Ts deceases with increasing Cu or Mn substitution, the superconducting state is gradually suppressed. It indicates that the driving force to the formation of low-temperature phase, the monoclinic $P112/n$ structure, could be the key for the formation of superconductivity in this type of superconductors.

It is worth noting that the low-temperature structural distortion is completed by elongation along the (110) direction of tetragonal cell, which is shown by an arrow in Fig. 3(a), revealing a one-dimension like pyramid chain through Se sites. It is natural to consider that Fermi-surface nesting along the (110) direction could be mediated with this anisotropic chain. In this regard, the Fermi-surface nesting along with phonon softening at proper temperatures could be an

important driving force for the structural distortion. Further measurements on single crystals should be conducted before making any definite conclusion.

In summary we report the strong suppression of superconductivity by Cu substitution in the FeSe system. Samples with Cu substitution over 3 at. % show no structural distortion and no superconductivity down to 2 K. In comparison with Mn substitution, we found that the inhibited tetragonal to monoclinic structural phase transition is responsible for the suppression of superconducting transition. Detailed structural analyses suggest that for the FeSe system the modification of $FeSe_4$ tetrahedron is essential to the structural phase transition and thus to the origin of superconductivity.

The authors acknowledge H. C. Su and C. H. Lee of the National Tsing-Hua University for their support on the neutron experiments. This work was partially supported by the National Science Council of Taiwan. We also acknowledge the National Synchrotron Research Radiation Centre in Taiwan and the U.S. AFOSR/AOARD for their financial support.

*twhuang@phys.sinica.edu.tw
†mkwu@phys.sinica.edu.tw

[1] Y. Kamihara, H. Hiramatsu, M. Hirano, R. Kawamura, H. Yanagi, T. Kamiya, and H. Hosono, J. Am. Chem. Soc. **128**, 10012 (2006).
[2] Y. Kamihara, T. Watanabe, M. Hirano, and H. Hosono, J. Am. Chem. Soc. **130**, 3296 (2008).
[3] H. Takahashi, K. Igawa, K. Arii, Y. Kamihara, M. Hirano, and H. Hosono, Nature (London) **453**, 376 (2008).
[4] X.-H. Chen, T. Wu, G. Wu, R. H. Liu, H. Chen, and D. F. Fang, Nature (London) **453**, 761 (2008).
[5] J. Zhao, Q. Huang, C. de la Cruz, S. Li, J. W. Lynn, Y. Chen, M. A. Green, G. F. Chen, G. Li, Z. C. Li, J. L. Luo, N. L. Wang, and P. Dai, Nature Mater. **7**, 953 (2008).
[6] M. Rotter, M. Tegel, and D. Johrendt, Phys. Rev. Lett. **101**, 107006 (2008).
[7] F.-C. Hsu, J.-Y. Luo, K.-W. Yeh, T.-K. Chen, T.-W. Huang, P. M. Wu, Y.-C. Lee, Y.-L. Huang, Y.-Y. Chu, D.-C. Yan, and M. K. Wu, Proc. Natl. Acad. Sci. U.S.A. **105**, 14262 (2008).
[8] K.-W. Yeh, T.-W. Huang, Y.-L. Huang, T.-K. Chen, F.-C. Hsu, P. M. Wu, Y.-C. Lee, Y.-Y. Chu, C. L. Chen, J.-Y. Luo, D.-C. Yan, and M. K. Wu, EPL **84**, 37002 (2008).
[9] Y. Mizuguchi, F. Tomioka, S. Tsuda, T. Yamaguchi, and Y. Takano, Appl. Phys. Lett. **93**, 152505 (2008).
[10] A. J. Drew, Ch. Niedermayer, P. J. Baker, F. L. Pratt, S. J. Blundell, T. Lancaster, R. H. Liu, G. Wu, X. H. Chen, I. Watanabe, V. K. Malik, A. Dubroka, M. Rossle, K. W. Kim, C. Baines, and C. Bernhard, Natue Mater. **8**, 310 (2009).
[11] C. de la Cruz, Q. Huang, J. W. Lynn, W. Jiying Li, I. I. Ratcliff, J. L. Zarestky, H. A. Mook, G. F. Chen, J. L. Luo, N. L. Wang, and P. Dai, Nature (London) **453**, 899 (2008).
[12] T. Nomura, S. W. Kim, Y. Kamihara, M. Hirano, P. V. Sushko, K. Kato, M. Takata, A. L. Shluger, and H. Hosono, Supercond. Sci. Technol. **21**, 125028 (2008).
[13] H. Luetkens, H.-H. Klauss, M. Kraken, F. J. Litterst, T. Dellmann, R. Klingeler, C. Hess, R. Khasanov, A. Amato, C. Baines, M. Kosmala, O. J. Schumann, M. Braden, J. Hamann-Borrero, N. Leps, A. Kondrat, G. Behr, J. Werner, and B. Buchner, Nature Mater. **8**, 305 (2009).
[14] S. A. J. Kimber, A. Kreyssig, Y.-Z. Zhang, H. O. Jeschke, R. Valenti, F. Yokaichiya, E. Colombier, J. Yan, T. C. Hansen, T. Chatterji, R. J. McQueeney, P. C. Canfield, A. I. Goldman, and D. N. Argyriou, Nature Mater. **8**, 471 (2009).
[15] K.-W. Yeh, H.-C. Hsu, T.-W. Huang, P. M. Wu, Y.-L. Huang, T.-K. Chen, J.-Y. Luo, and M. K. Wu, J. Phys. Soc. Jpn. Suppl. C **77**, 19 (2008).
[16] M. K. Wu, F.-C. Hsu, K.-W. Yeh, T.-W. Huang, J.-Y. Luo, M.-J. Wang, H.-H. Chang, T.-K. Chen, S.-M. Rao, B.-H. Mok, C. L. Chen, Y.-L. Huang, C.-T. Ke, P. M. Wu, A.-M. Chang, C.-T. Wu, and T. P. Perng, Physica C **469**, 340 (2009).
[17] K. Ishida, Y. Nakai, and H. Hosono, J. Phys. Soc. Jpn. **78**, 062001 (2009).
[18] J. A. Wilson, J. Phys.: Condens. Matter **22**, 203201 (2010).
[19] T. M. McQueen, Q. Huang, V. Ksenofontov, C. Felser, Q. Xu, H. Zandbergen, Y. S. Hor, J. Allred, A. J. Williams, D. Qu, J. Checkelsky, N. P. Ong, and R. J. Cava, Phys. Rev. B **79**, 014522 (2009).
[20] T. M. McQueen, A. J. Williams, P. W. Stephens, J. Tao, Y. Zhu, V. Ksenofontov, F. Casper, C. Felser, and R. J. Cava, Phys. Rev. Lett. **103**, 057002 (2009).
[21] I. I. Mazin, M. D. Johannes, L. Boeri, K. Koepernik, and D. J. Singh, Phys. Rev. B **78**, 085104 (2008).
[22] T. Imai, K. Ahilan, F. L. Ning, T. M. McQueen, and R. J. Cava, Phys. Rev. Lett. **102**, 177005 (2009).
[23] B.-L. Young, J. Wu, T.-W. Huang, K.-W. Yeh, and M. K. Wu, Phys. Rev. B **81**, 144513 (2010).
[24] W. A. MacFarlane, O. Ofer, K. H. Chow, M. D. Hossain, T. J. Parolin, H. Saadaoui, Q. Song, D. Wang, J. Sugiyama, D. J. Arseneau, B. Hitti, K.-W. Yeh, and M. K. Wu (unplublished).
[25] S. Matsuishi, Y. Inoue, T. Nomura, Y. Kamihara, M. Hirano, and H. Hosono, New J. Phys. **11**, 025012 (2009).
[26] A. S. Sefat, R. Jin, M. A. McGuire, B. C. Sales, D. J. Singh, and D. Mandrus, Phys. Rev. Lett. **101**, 117004 (2008).
[27] J. H. Chu, J. G. Analytis, C. Kucharczyk, and I. R. Fisher, Phys. Rev. B **79**, 014506 (2009).
[28] A. J. Williams, T. M. McQueen, V. Ksenofontov, C. Felser, and R. J. Cava, J. Phys.: Condens. Matter **21**, 305701 (2009).
[29] K. D. Liss, B. A. Hunter, M. E. Hagen, T. J. Noakes, and S. J. Kennedy, Physica B **385-386**, 1010 (2006).
[30] A. J. Studer, M. E. Hagen, and T. J. Noakes, Physica B **385-386**, 1013 (2006).
[31] C. Chen, S. Rao, C. Dong, J. Chen, T. Huang, B. Mok, M. Ling, W. Wang, C. Chang, T. Chan, J. Lee, J. Guo, and M. Wu, arXiv:1005.0664 (unpublished).
[32] A. Kisiel, A. Kisiel, P. Zajdel, P. M. Lee, E. Burattini, and W. Giriat, J. Alloys Compd. **286**, 61 (1999).
[33] B. H. Mok, S. M. Rao, M.-C. Ling, K.-J. Wang, C.-T. Ke, P. M. Wu, C.-L. Chen, F.-C. Hsu, T.-W. Huang, J.-Y. Luo, D.-C. Yan,

K.-W. Yeh, T.-B. Wu, A.-M. Chang, and M. K. Wu, Cryst. Growth Des. **9**, 3260 (2009).
[34] K.-W. Lee, V. Pardo, and W. E. Pickett, Phys. Rev. B **78**, 174502 (2008).
[35] E. Pomjakushina, K. Conder, V. Pomjakushin, M. Bendele, and R. Khasanov, Phys. Rev. B **80**, 024517 (2009).
[36] M. Bendele, A. Amato, K. Conder, M. Elender, H. Keller, H.-H. Klauss, H. Luetkens, E. Pomjakushina, A. Raselli, and R. Khasanov, Phys. Rev. Lett. **104**, 087003 (2010).